Effects of internal resonances in the pitch glide of Chinese gongs

Marguerite Jossic[a)]
Sorbonne Université, CNRS, Institut Jean Le Rond d'Alembert, F-75005 Paris, France

Olivier Thomas[b)] and Vivien Denis
Arts et Métiers Paristech, LISPEN EA 7515, 8 bd. Louis XIV, 59046 Lille, France

Baptiste Chomette
Sorbonne Université, CNRS, Institut Jean Le Rond d'Alembert, F-75005 Paris, France

Adrien Mamou-Mani and David Roze
STMS UMR 9912, Sorbonne Université, CNRS, Ircam, 1 place Igor Stravinsky, F-75004 Paris, France

The framework of nonlinear normal modes gives a remarkable insight into the dynamics of nonlinear vibratory systems exhibiting distributed nonlinearities. In the case of Chinese opera gongs, geometrical nonlinearities lead to a pitch glide of several vibration modes in playing situation. This study investigates the relationship between the nonlinear normal modes formalism and the ascendant pitch glide of the fundamental mode of a xiaoluo gong. In particular, the limits of a single nonlinear mode modeling for describing the pitch glide in playing situation are examined. For this purpose, the amplitude-frequency relationship (backbone curve) and the frequency-time dependency (pitch glide) of the fundamental nonlinear mode is measured with two excitation types, in free vibration regime: first, only the fundamental nonlinear mode is excited by an experimental appropriation method resorting to a phase-locked loop; second, all the nonlinear modes of the instrument are excited with a mallet impact (playing situation). The results show that a single nonlinear mode modeling fails at describing the pitch glide of the instrument when played because of the presence of 1:2 internal resonances implying the nonlinear fundamental mode and other nonlinear modes. Simulations of two nonlinear modes in 1:2 internal resonance confirm qualitatively the experimental results.

I. INTRODUCTION

Musical instruments from the percussion family exhibit various nonlinear features which are typically those encountered in plates, shells, and beams when geometrical nonlinearities are present:[1] amplitude-frequency dependence, internal resonances (strong energy coupling between modes), harmonic distortion, and chaos are some typical nonlinear features that can be observed in such structures.[2] In the case of Chinese opera gongs, amplitude-frequency dependence can be considered as a true musical pattern:[1] the frequency changes as the vibration decreases, which is highlighted by a very characteristic "pitch glide" in playing situation. The amplitude-frequency dependence can be either of softening type—frequency increases with time in free vibration (*xiaoluo* gong)—or hardening type—frequency decreases with time in free vibration (*daluo* gong).

Surprisingly, only four studies have been carried out about Chinese opera gongs: Rossing and Fletcher[3] experimentally studied the influence of radial tension or compression on the type of nonlinearity (hardening or softening). Fletcher[4] showed that the pitch glide phenomenon depends on the ratio between the thickness of the gong and the height of its central shell. Tsai *et al.*[5] performed an experimental and numerical linear analysis of a *daluo*. Jossic *et al.*[6] underlined the presence of internal resonances in the *xiaoluo* using modal active control. This small interest is all the more surprising since, as it will be shown, a single Duffing oscillator is sufficient to describe the frequency-amplitude dependence; in contrast, many degree-of-freedom models are required to describe internal resonances and/or chaos phenomena, which have received considerable interest in the case of gongs and cymbals[7–10] or the steelpan.[11,12]

Many previous studies on plates and shells (see, e.g., Refs. 1, 2, and 13) have highlighted that geometrical nonlinearities lead to quadratically and/or cubically coupled modal equations; conversely, the linear case is characterized by uncoupled modal equations. In the nonlinear range, such couplings are responsible for the loss of the linear eigenspace invariance property, which in turn hinders finding nonlinear reduced order models. In particular, truncating directly the modal equations, i.e., keeping only one non-zero modal coordinate in the equations, may lead to erroneous results in the prediction of the nonlinearity trend.[14–16]

The concept of nonlinear modes allows us to overcome some of these difficulties. The formalism relies on the normal form theory[16,17] which enables the reduction of the nonlinear dynamics to invariant manifolds in the phase space, by a nonlinear change of variables of the initial (linear) modal coordinates. Each invariant manifold in the phase space corresponds to a *nonlinear normal mode* and is tangent to the linear

[a)]Also at: STMS 9912, Sorbonne Université, CNRS, Ircam, 1 place Igor Stravinsky, F-75004 Paris, France.
[b)]Electronic mail: olivier.thomas@ensam.eu

corresponding eigenspace at the equilibrium point. When there is no internal resonance in the system dynamics, the behavior of the system can be described by a single nonlinear mode which is able to efficiently capture the nonlinearity trend (hardening/softening).

In this context, this paper investigates the relevance and limits of a single nonlinear mode modeling to describe the pitch glide of the fundamental mode of a *xiaoluo* gong in playing situation. In particular, one can wonder if the presence of internal resonances in these instruments[6] may impact the frequency-amplitude behavior leading to the characteristic pitch glide. For this purpose, this study compares the frequency-amplitude relationship (backbone curve) and frequency-time dependence (pitch glide) of the gong fundamental mode in free vibration in two experiments: (i) in the case of a single nonlinear mode excitation in a frequency range that avoids the appearance of internal resonances and (ii) in playing situation, where several nonlinear modes are excited and internal resonances may occur.

Two main techniques have been recently used for the measurement of backbone curves. First, the nonlinear phase resonance testing (NPR) is an extension of linear phase resonance testing[18] for nonlinear systems, and consists in (i) setting the system to a phase resonance for a given (nonlinear) mode by the mean of force appropriation,[19] and (ii) turning off the excitation and measuring the free decay vibration regime. For lightly damped systems, the invariance property guarantees that the free regime stays on the conservative nonlinear mode manifold.[19] The backbone curve is then extracted from the free vibration regime using time-frequency analysis. The second and more recent technique is referred to as experimental continuation, a concept that is inspired by numerical continuation methods. The first continuation technique is the control-based continuation[20,21] that uses a combination of a stabilizing feedback control and a path-following method. In the second continuation technique, which is used in this study, the tracking of the backbone is carried out in forced regime by setting the system at phase resonance using a phase-locked-loop (PLL) controller.[22–25] The forcing amplitude is set incrementally step by step and the forcing frequency is adjusted by the PLL in order to achieve the nonlinear phase resonance. The main advantage of continuation techniques is to directly obtain the backbone curve from forced regime rather than rely on the free vibration frequency-time analysis, which is performed with the NPR method.

In the first experiment, we combine nonlinear phase resonance testing and a PLL system to measure the backbone curve and the frequency-time dependence of the nonlinear fundamental mode of a *xiaoluo*. More precisely, the nonlinear mode appropriation is realized in forced regime using the PLL setup. Then, the excitation is stopped and the frequency-amplitude-time relationships are extracted from free decay, as in the nonlinear phase resonance testing. The main reason for using the free vibration regime is to avoid thermal effects that are induced by high-amplitude forced vibration at resonance. These effects will be experimentally demonstrated. Results from the first experiment are compared with estimation of the same frequency-amplitude-time curves obtained from mallet-strike excitation in the second experiment.

The paper is organized as follows: Section II provides some background on the nonlinear mode formalism and the PLL principle. Section III presents the experimental setup for the two experiments. Measurements of the backbone curve and associated thermal effects are reported in Sec. IV. Empirical evidence of internal resonances is then presented in Sec. V and are qualitatively assessed by simulations. Finally, some conclusions and perspectives are given in Sec. VI.

II. THEORY AND METHODS

A. Background on nonlinear modes

Only the main ideas are proposed here and the interested reader can refer to Refs. 24 and 25 for further details. We consider the gong as an elastic shell with large amplitude vibration and thus subjected to geometrical nonlinearities. The transverse displacement $w(\boldsymbol{x},t)$ at time t and position $\boldsymbol{x}$ is expanded in a family of N eigenmodes of the linearized model:

$$w(\boldsymbol{x},t)=\sum_{k=1}^{N}\Phi_k(\boldsymbol{x})q_k(t), \tag{1}$$

where $[\omega_k,\Phi_k(\boldsymbol{x})]$ are the kth natural angular frequency and mode shape. The modal coordinates $q_k(t)$ satisfy the following set of coupled nonlinear equations, for all $k=1,\ldots N$:

$$\ddot{q}_k+\omega_k^2q_k+\sum_{i,j=1}^{N}\beta_{ij}^kq_iq_j+\sum_{i,j,l=1}^{N}\gamma_{ijl}^kq_iq_jq_k=0, \tag{2}$$

where β_{ij}^k and γ_{ijl}^k are nonlinear coefficients stemming from the geometrical nonlinearities. Here, only the conservative unforced case is considered.

Using normal forms, as introduced in Refs. 14, 16, and 17, it is possible to simplify model (2) by introducing the following nonlinear change of coordinates, for all $k=1,\ldots N$:

$$q_k=u_k+\mathcal{P}_k^{(2)}(u_i,\dot{u}_i)+\mathcal{P}_k^{(3)}(u_i,\dot{u}_i), \tag{3}$$

where $\mathcal{P}_k^{(p)}(u_i,\dot{u}_i)$, $i=1,\ldots N$, is a polynomial function of $(u_i,\dot{u}_i)$ containing monomial terms of order p only. A new dynamical system, a function of the normal coordinates $u_k(t)$, is obtained, which has two properties: (i) it has fewer nonlinear coupling terms than the initial one [Eq. (2)] and (ii) each so-called normal oscillator is invariant if it is not involved in an internal resonance with another one. The latter property enables the association of each normal oscillator to a nonlinear normal mode (NNM).[14,25–27] It also means that in free vibrations, if the motion is initiated on the kth normal oscillator, no energy is transferred to the others. In this particular case, namely, if a motion on the ith NNM is considered, then $u_j=0,\dot{u}_j=0,\ \forall j\neq i$, and the dynamics of the system is thus equivalent to

$$\ddot{u}_i+\omega_i^2u_i+\Gamma_1u_i^3+\Gamma_2u_i\dot{u}_i^2=0, \tag{4}$$

where (Γ_1,Γ_2) are two coefficients depending on the nonlinear coefficients β_{ij}^k and γ_{ijl}^k of the initial dynamical system [Eq. (2)], that take into account the influence of other linear modes in the dynamics of the considered ith NNM.[14]

A first order perturbation solution of Eq. (4) leads to

$$u_i(t) = a\cos(\omega_{\mathrm{nl}}t + \varphi), \tag{5}$$

with[14]

$$\omega_{\mathrm{nl}} = \omega_i(1 + Ta^2) \quad \text{and} \quad T = \frac{3\Gamma_1 + \Gamma_2\omega_i^2}{8\omega_i^2}. \tag{6}$$

It shows that to first order, the oscillations of a given NNM are harmonic with a frequency ω_{nl} that depends on the amplitude a of the motion. The so-called backbone curve is obtained by plotting ω_{nl} as a function of a.[2]

In practice, the T coefficient can be experimentally identified, but afterwards it is no longer possible to identify separately the coefficients Γ_1 and Γ_2. Moreover, numerical simulations of Eq. (4), with several values of (Γ_1, Γ_2) that lead to the same value of T, show that for moderate amplitudes, all backbone curves are merged into a single parabola defined by Eq. (6). This result is valid for values of a corresponding to a change of frequency ω_{nl} less than 10% (Ref. 25)—this condition will be satisfied in our experiments (see Sec. II C). Consequently, we propose to approximate the dynamics of a given NNM by a single Duffing oscillator:

$$\ddot{u}_i + \omega_i^2 u_i + \tilde{\Gamma}_0 u_i^3 = 0, \tag{7}$$

with

$$\tilde{\Gamma}_0 = \frac{8\omega_i^2 T}{3} = \Gamma_1 + \frac{\Gamma_2\omega_i^2}{3}. \tag{8}$$

In order to obtain the expression in the physical space of the NNM described in Eq. (7), we replace the expression (5) in the nonlinear change of variables in Eq. (3). To first order, one obtains[25]

$$w(\boldsymbol{x}, t) \simeq \Phi_i(\boldsymbol{x})u_i(t).$$

This last equation allows the NNM to be rewritten in physical space,

$$\ddot{w} + \omega_i^2 w + \Gamma_0 w^3 = 0, \tag{9}$$

with

$$\Gamma_0 = \tilde{\Gamma}_0\Phi_i^2(\boldsymbol{x}).$$

This last equation shows that if Eq. (9) is used for the experimental identification of the NNM, it leads to a value Γ_0 of the nonlinear coefficient that depends on the location $\boldsymbol{x}$ where the displacement $w(\boldsymbol{x}, t)$ is measured. Otherwise, it is necessary to correct it by taking into account the mode shape $\Phi_i(\boldsymbol{x})$ to estimate $\tilde{\Gamma}_0$ of Eq. (7).

B. Backbone identification

1. Nonlinear phase resonance testing

The rigorous formalism of NNM recalled in Sec. II A has recently contributed to the development of new nonlinear modal identification techniques based on backbone curve measurement. Among them, the NPR method extends the concept of linear phase resonance[28] to nonlinear systems, and allows for excitation and identification of single NNMs. For a given driven single oscillator, phase resonance occurs when the excitation term exactly cancels, for all time t, the damping of the system: in this case, the oscillator behaves as if it was in undamped free oscillations. For a linear oscillator, it is well known[28] that phase resonance is achieved when the excitation is in phase quadrature with the system displacement. In the nonlinear case, the system response is often multiharmonic and phase resonance is obtained by balancing each harmonic of the damping term by a corresponding harmonic in the forcing.[19]

The NPR method has been first detailed by Peeters *et al.*[19] and follows a two-step process. First, the system is driven to a single nonlinear mode phase resonance by applying a multipoint harmonic excitation at the mode natural frequency. The quality of the nonlinear mode appropriation is theoretically guaranteed by a phase quadrature indicator, which is valid for linear systems and has been proved to be generalizable to nonlinear systems.[19] In practice, even an imperfect force appropriation resulting from a single-point mono-harmonic excitation may be sufficient for the NNM appropriation.[19] This approximation proves to be relevant as all the harmonics higher than the fundamental governing the NNM dynamics can be neglected.[25] Therefore, the phase resonance can be achieved experimentally by ensuring the phase quadrature on the first harmonic only.[25] When the phase resonance is reached, the applied excitation compensates for the damping forces. As a result, the structure vibrates according to the NNM of the underlying conservative system.

In a second stage, the excitation is turned off and the free decay response of the NNM is measured. Due to the invariance property of NNMs the system free vibration follows the nonlinear normal mode of the damped system. Specifically, in the case of lightly damped systems such as gongs,[6] the dynamics of the damped NNM closely follows the underlying conservative NNM, whose dynamics is governed by Eq. (7).[16] Tracking of the frequency-amplitude behavior of the free damped regime by time-frequency analysis is then performed in order to compute the backbone curve of the associated NNM.

The NPR method has proved its robustness and accuracy in various experimental studies[19,29,30] and is therefore widely used for nonlinear modal testing. The problem of NNM appropriation in the case of internal resonances was also addressed in Ref. 31. The principal disadvantage of the method lies in the excitation tuning: as the level of excitation energy increases, jump phenomena may occur in the system frequency response leading to a time-consuming tuning of the excitation.

2. PLL controller

The issue of excitation tuning has recently been overcome by experimental continuation techniques for backbone curve measurements. Among them, a major contribution has been made with the use of PLL controllers.[32] The approach is based on the fact that phase-controlled self-excited systems do not exhibit unstable behavior of the vibration amplitude.[25,33] More specifically, the amplitude-phase curve of single-degree-of-

freedom systems is single-valued and flat near the resonance for many nonlinear systems, contrary to the traditional jump phenomenon encountered in the amplitude-frequency relationship. This property remains valid as long as the frequency and amplitude ranges do not allow for internal resonances.[23]

PLL controllers are designed in order to guarantee a given phase lag between the forcing excitation of a system and a reference signal (e.g., the system response: displacement, velocity). More precisely, a PLL adjusts the forcing excitation frequency (control command) in order to keep the phase lag to a preset value. The phase lag value can be either variable with time or fixed. In the first configuration, sweeping the phase lag value over the range [0–π] while keeping the excitation force constant allows for the reconstruction of the *complete* frequency-amplitude curves of the NNM, thanks to the monotony of the frequency-phase relationship.[22,25] In the second configuration, setting the phase lag value at 0 or $\pi/2$ (depending on whether we measure the NNM velocity or displacement, respectively) allows for the tracking of the backbone curve (nonlinear phase resonance).[23] This latter configuration is used in the study.

The PLL controller consists of a phase detector, a proportional–integral–derivative controller (PID), and a voltage controlled oscillator (VCO)[23,34] (see Fig. 1). The overall PLL system is the same as the one previously developed in Ref. 25. The first step consists of choosing an initial forcing excitation amplitude F, an initial forcing frequency $\omega = \omega_0$, and a fixed phase lag command ϕ_{ref}. The nonlinear mode response x_m is measured along with the forcing excitation F_m. The phase detector determines the phase shift ϕ between x_m and F_m using a synchronous demodulation[34] that estimates the fundamental harmonic of x_m and F_m from the forcing excitation. The error e between the phase ϕ and the phase command ϕ_{ref} is then integrated by an integral controller which gives a correction to the initial forcing frequency ω_0. The new forcing frequency is determined by the voltage controlled oscillator and leads to a new forcing excitation for the system. Note that the excitation amplitude F is kept constant during this process. The construction of the backbone curve is realized by iterating the process for increasing excitation amplitudes F: at each amplitude step, the phase controller adjusts the excitation frequency in order to meet the phase resonance criterion ϕ_{ref}.

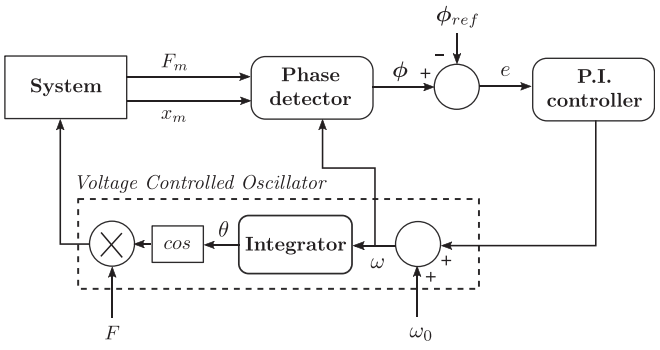

FIG. 1. Phase-locked loop principle. The forcing amplitude F, the phase lag ϕ_{ref}, and the initial pulsation ω_0 are defined by the user. Please refer to the main text for the detailed description of the system.

C. Study protocol

Two experiments are carried out to test the validity of single NNM modeling for the description of the pitch glide in playing conditions.

The first experiment (experiment A) measures the gong fundamental mode response in free vibration regime in the case of *single NNM excitation*. This is achieved by performing the fundamental nonlinear mode appropriation with the PLL controller. The single NNM appropriation is guaranteed by setting the initial forcing amplitude at a level that does not allow for internal resonances. For this reason, the experiment is performed over a limited frequency range (440−449 Hz). Beyond this frequency range, the frequency shift of the nonlinear normal mode allows for the appearance of 1:2 internal resonances between the nonlinear fundamental mode and other linear modes (see Sec. V), breaking the single NNM appropriation. Once the phase resonance is achieved using the PLL controller, the excitation is shut down and the free vibration regime of the single fundamental NNM is measured. The backbone curve and the frequency-time relationship are then extracted from the free vibration measurements.

The second experiment (experiment B) is carried out in a playing situation: the gong is struck with various mallet impacts. The pitch glide and the backbone curve of the fundamental nonlinear mode are extracted from the free vibration data, and compared to the results of experiment A.

In both experiments, frequency-time post-processing is performed to extract the amplitude-frequency curve (backbone curve) and the frequency-time curve (pitch glide) from the fundamental free vibration regime. The measurement of the backbone curve in the free vibration regime using the PLL setup set the first experiment (experiment A) a bit apart from the previous PLL backbone curve measurements[23,25] where the backbone curves were measured in forced regime. This *a priori* choice avoids thermal effects evidenced in Sec. IV C. The details about the two experiments are given in Sec. III.

III. EXPERIMENTAL SETUPS

The setup of experiment A is displayed in Fig. 2. The Chinese gong (approximately ∼220 mm large and 1 mm thick) is excited with a homemade coil-magnet system fully described in Ref. 35 [Fig. 3(a)] preceded by a power amplifier (B&K 2719). The magnet is located on the edge of the gong central area in order to (i) provide an efficient excitation of the fundamental mode located in the center of the instrument[6] and

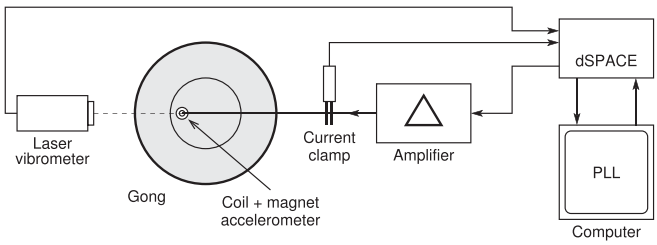

FIG. 2. Setup for experiment A (PLL measurements, single nonlinear mode excited).

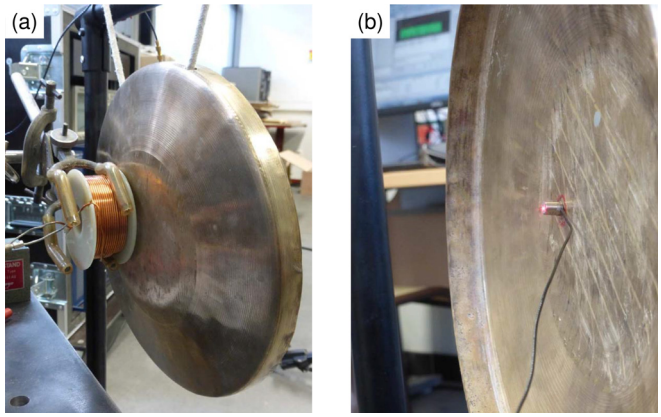

FIG. 3. (Color online) Instrumentation of the gong. (a) Front of the *xiaoluo* gong with magnet-coil system. (b) Back of the gong with the accelerometer co-localized with the laser vibrometer.

(ii) minimize the change of the fundamental mode frequency stemming from the added mass of the magnet. The excitation force is proportional to the current in the coil and is measured by a current clamp. In order to keep the same instrumentation in both experiments, the accelerometer used in experiment B is also taped on the back of the instrument, co-localized with the magnet [Fig. 3(b)]. The velocity is measured by a laser vibrometer (Polytec PSV-400) at the same location as the accelerometer, so that the instrument responses can be compared between the two experiments. The PLL control diagram is implemented using Matlab/Simulink, and the overall phase control is driven by a DSpace MicroLabBox working at 10 000 Hz. First, the system is set at phase resonance using the PLL controller. This is done by setting a relatively high excitation amplitude, and waiting for the PLL to adjust the forcing frequency in order to meet the resonance phase criterion ϕ_{ref}. As we measure the nonlinear fundamental mode velocity, $\phi_{\text{ref}} = 0$. Then, the excitation is stopped, and the free decay vibration of the fundamental mode is measured. The backbone curve and the frequency-time dependency are extracted from the vibrometer data spectrograms.

The experiment B setup is represented in Fig. 4. The gong is struck with various impact forces and impact locations using a mallet. The nonlinear normal mode acceleration is measured with the accelerometer (B&K 4374) pictured in Fig. 3(b). The use of an accelerometer for experiment B is mandatory since the movements of the instrument prevents the vibrometer from correctly measuring the system velocity. Another accelerometer (B&K 4374) is taped to the mallet stick [Fig. 5(a)] and is calibrated in order to recover the impact force. The calibration is realized by measuring the impact force of 50 mallet strikes on a PCB 208C02 force sensor [Fig. 5(b)]. The ratio between

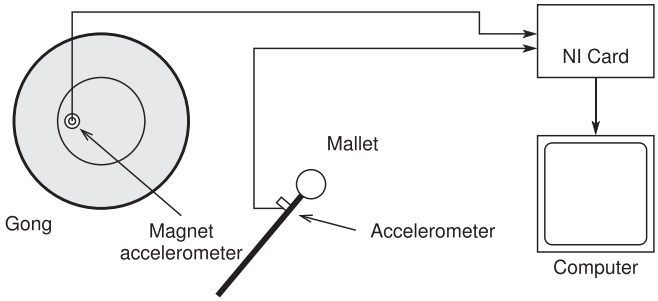

FIG. 4. Setup for experiment B (mallet measurements, several nonlinear modes excited).

the force sensor and the accelerometer signals corresponding to an equivalent mass revealed to be approximately constant (∼3 kg) whatever the mallet impact force amplitude. The mean of the equivalent mass measured for all the different mallet impacts is used to recover the impact force from the mallet accelerometer signal. This is exemplified in Fig. 6, where the impact force measured by the force sensor (blue line) is compared to the reconstructed force obtained by the accelerometer signal multiplied by the mean equivalent mass (red line). The pale red area represents the standard deviation of the reconstructed force due to the standard deviation of the equivalent mass calculation. Note that the impact force is included in the standard deviation of the reconstruction force, for both small value (∼6N) and high value (∼95N). The main parameters of experiment A and experiment B are summarized in Table I.

IV. RESULTS: PITCH GLIDE AND NONLINEAR MODE IDENTIFICATION

A. Pitch glide of the fundamental mode

The pitch glide of the gong fundamental mode is highlighted in playing situation by striking the instrument with increasing mallet forces (experiment B). Figure 7 shows four spectrograms of the accelerometer signal for increasing mallet impact forces F ($F = 8$N, $F = 13$N, $F = 16$N, $F = 32$N). These spectrograms highlight two points. First, one can see that the frequency-time dependence of the fundamental mode (around 450 Hz, black solid line in Fig. 7), which is absent from the instrument response for a small impact force ($F = 8$N), starts to appear from $F = 13$N, and gets larger as the impact force increases. The change of frequency versus time is directly related to (i) the combination of the frequency-amplitude phenomenon due to geometrical nonlinearities and (ii) the damping of the system. It is also responsible for the characteristic "pitch glide" one can hear when the instrument is played. The

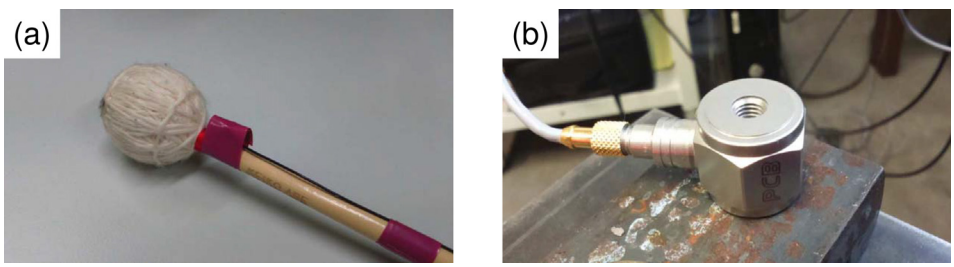

FIG. 5. (Color online) Instrumentation for mallet calibration: (a) mallet instrumented with an accelerometer and (b) force sensor.

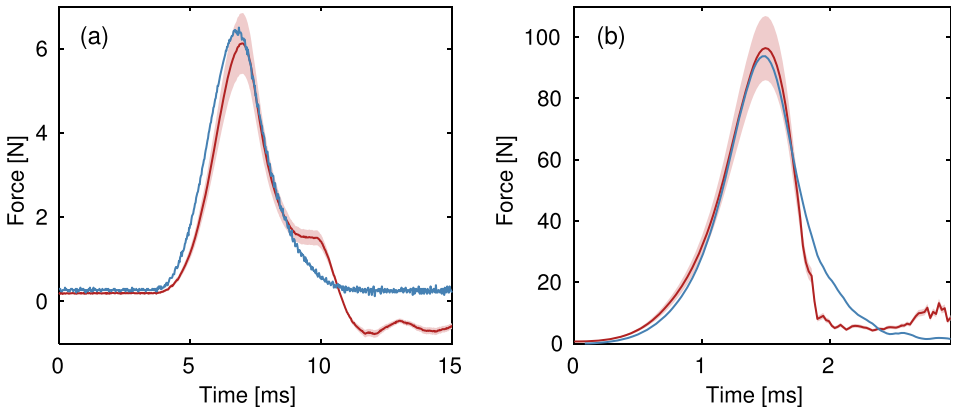

FIG. 6. (Color online) Results of mallet calibration. Measured force (blue line) and reconstructed force (red line) are compared. Pale red area represents the standard deviation of the reconstructed force. (a) Low energy mallet strike (∼6N) (b) High energy mallet strike (∼95N).

frequency-amplitude behavior of the nonlinear mode associated to the fundamental mode is measured by experiment A and the associated results will be exposed in Sec. IV B.

Second, the frequency of second harmonic distortion around 900 Hz (black dotted line in Fig. 7) which is twice the one of the fundamental mode, glides also upward and goes through two other linear modes at 859 and 880 Hz (displayed in red dot lines in Fig. 7). The experimental operational deflection shapes of the fundamental mode and these two modes were recorded from a modal analysis performed with the vibrometer used in Sec. III, and are shown in Fig. 8. This suggests the presence of a 1:2 internal resonance ($f_2 = 2f_1$) between the fundamental mode at 447 Hz and the modes at 859 and 880 Hz, which are, respectively, called mode 1, mode 2, and mode 3 in the following. Other modes present in the modal analysis and visible in Fig. 7 (e.g., the mode at 811 Hz) are not numbered since they are not involved in an internal resonance with the fundamental mode. The effects of the internal resonances between modes 1, 2, and 3 will be further exposed in Sec. V.

B. Nonlinear mode identification

For experiments A and B, the backbone curves (amplitude-frequency relationship) of the NNM were extracted from the spectrogram of the free vibration regime. The (amplitude, frequency) couple of the NNM is obtained as follow: for each time, the amplitude is estimated by taking the maximum amplitude of the spectrogram in the frequency window 400−500 Hz around the fundamental harmonics of the signal, corrected by taking into account the length of the time window of the short time Fourier transform; the corresponding instantaneous frequency is then taken as equal to the window maximum frequency. Computing the spectrogram was done from vibrometer data in the case of experiment A, and from accelerometer data for experiment B. The resulting velocity and acceleration backbone curves were then divided once or twice by the pulsation axis, respectively, in order to obtain the backbone curves in displacement. In Fig. 9, the backbone curve corresponding to experiment A is plotted along with a standard deviation which corresponds to the standard deviation of five other PLL backbone curves measured at different times during the experimental process. Here two points should be emphasised. First, it is worth noticing that geometrical nonlinearities in spherical shells appear when the absolute value of the displacement is of the same order of h^3/d^2 or h^2/d, where h is the thickness of the shell and d its radius.[13] In our case, the values of the thickness and the radius of the gong are $h = 1$ mm and $d = 110$ mm. This leads to $h^2/d \sim 10^{-2}$ mm, which is at the same order of the transverse displacement measured in Fig. 9. This confirms the presence of geometrical nonlinearities in the gong. Second, Fig. 9 shows that the values of the backbone curve measured in experiment B are contained in the standard deviation of the backbone curves measured in experiment A. This result highlights that, in a few Hertz frequency range around the modal frequency, the fundamental nonlinear mode is able to describe the frequency-amplitude behavior of the *xiaoluo* in free vibration regime. This result also demonstrates the link between the fundamental pitch glide in Chinese gongs and the nonlinearity trend of the associated nonlinear mode. This latter fact is an important result since it has never been rigorously demonstrated in the literature on Chinese opera gongs.

The nonlinear coefficient Γ_0 of the nonlinear mode characterized by Eq. (9) can also be identified using a second order polynomial fit of the frequency-amplitude relationship [see Eq. (6)]. The result of the polynomial fit is represented with a red dot line in Fig. 9. The estimation of Γ_0 gives $\Gamma_0 = -8.1 \times 10^7$ mm^{-2}s^{-2}. Notice that, as explained at the end of Sec. II A, the above value of Γ_0 depends on the measuring point, here at the edge of the gong central area.

TABLE I. Summary of the excitation characteristics, the number of modes excited and the nonlinear mode response measurement for experiment A and experiment B.

Experiment	A	B
Excitation type	Forcing excitation	Impulse
Excitation system	Coil-magnet system	Mallet
Numb. of modes excited	$n = 1$	$n > 1$
Response measurement	Vibrometer	Accelerometer

C. Thermal effects in the coil-magnet system

This section underlines the thermo-mechanical effects encountered in the experiments when measuring the backbone curves with the PLL setup. These thermal effects made the backbone curve measurements delicate and justify that the measures were performed in free vibration regime instead of forced regime, as explained in the protocol (see Sec. II C). The main drawbacks of PLL backbone curve measurements

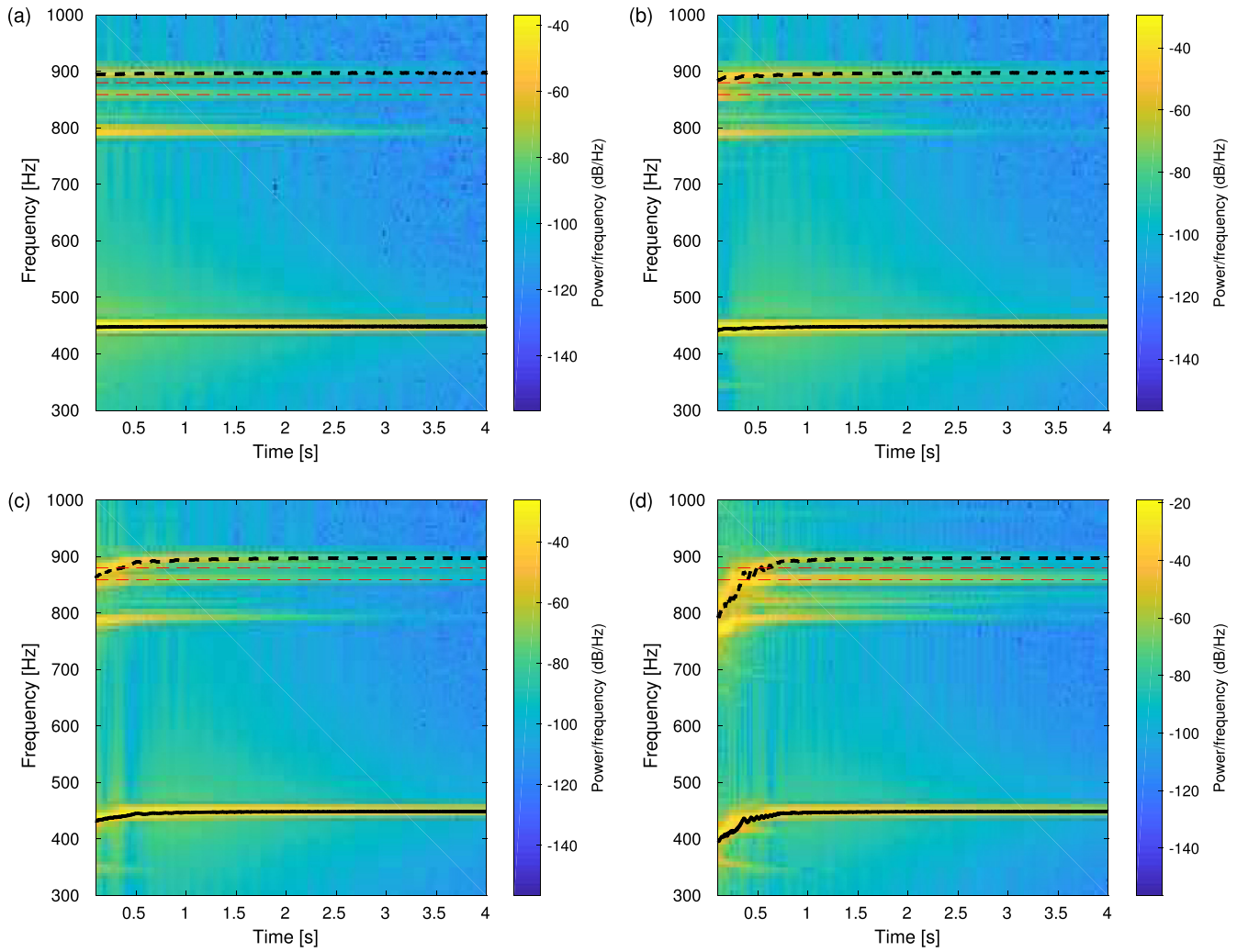

FIG. 7. (Color online) Spectrograms of the accelerometer signal, for increasing mallet impact forces F. The instantaneous frequency of the fundamental mode acceleration (experimental, bold dark line), its quadratic harmonic distortion (dash dark line, plotted by multiplying by two the frequency of the fundamental), and the modes at 859 and 880 Hz which are supposed linear (theoretical, dashed red lines), are also plotted for easy readability. (a) $F = 8$N, (b) $F = 13$N, (c) $F = 16$N, (d) $F = 32$N.

in forced vibration is that the process is longer than in free vibration ($\sim$3 min in forced regime versus $\sim$30 s in free vibration). As a consequence, the coil-magnet system, which is used during the whole experiment, is more likely to heat-up. This is illustrated in Fig. 10, where three different backbone curves have been measured at different amplitudes. Each plot corresponds to a two step experiment: first, the backbone curve is measured in forced vibration until a maximum forcing amplitude (black solid line). Second, the forcing excitation is stopped and the system goes back to zero in free vibration (black dot line). In the first step, the system dynamics stands on the conservative NNM manifold, whereas in the second step, it follows the damped NNM manifold. As the viscous damping of the fundamental mode is small ($\sim$0.1%, see Ref. 6), the frequency-amplitude curves obtained in the two steps should be the same.[16] However, one

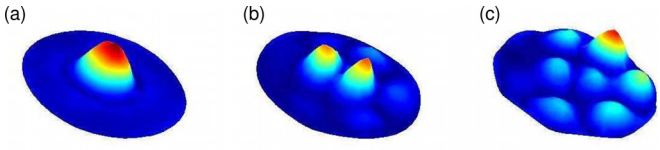

FIG. 8. (Color online) Experimental operational deflection shapes of the linear modes involved in a 1:2 internal resonance. (a) Mode 1: axisymmetric mode (0,1) at 447 Hz. (b) Mode 2: asymmetric mode (1,1) at 859 Hz. (c) Mode 3: asymmetric mode (7,1) at 880 Hz.

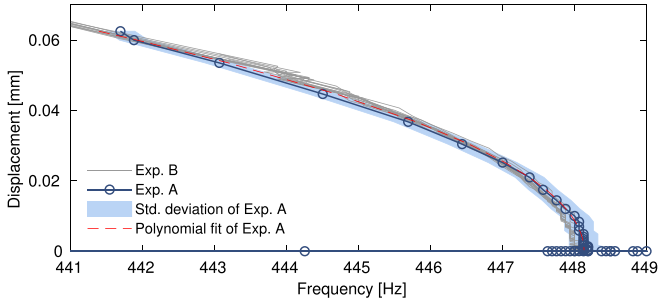

FIG. 9. (Color online) Backbone curves of the fundamental nonlinear mode obtained from the free vibration regime in experiment A (PLL system, blue circles) and in experiment B (mallet strikes, 15 data sets, grey lines). The standard deviation of experiment A is indicated with a light blue area. The polynomial fit performed on the backbone curve of experiment A is also represented with a red dot line.

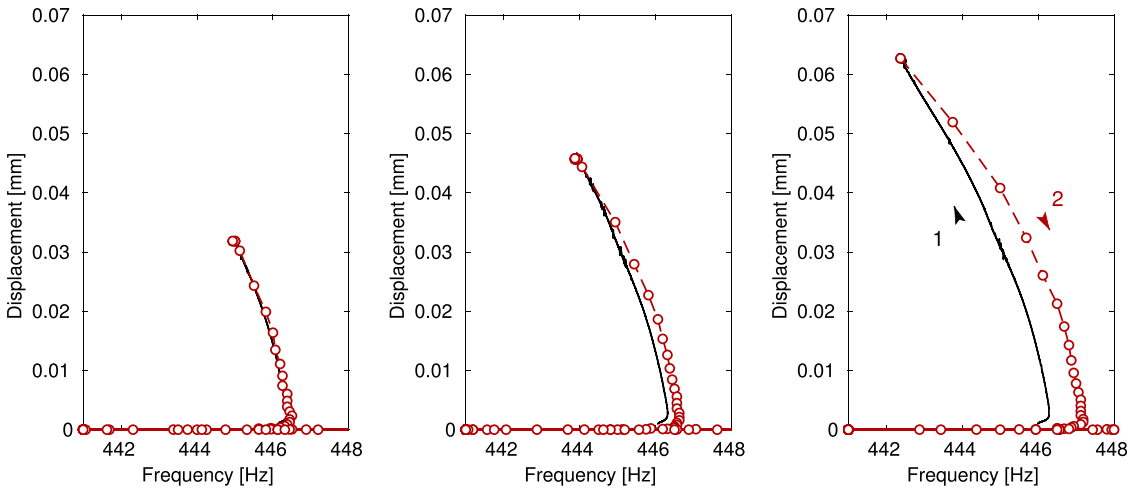

FIG. 10. (Color online) Backbone curves obtained successively with the PLL setup in forced regime at phase resonance (equivalent to the undamped system, black solid line, step ①) and in free regime (red circles, step ②), for increasing amplitude levels.

can see that it is not always the case. For small vibration backbone curves, the two curves are identical [Fig. 10(a)]. But as the maximum amplitude of the backbone curve increases, one can see that the frequency-amplitude curves are not the same in forced regime and in free vibration regime [Figs. 10(b) and 10(c)]. The higher the backbone amplitude, the greater the frequency shift between the two curves.

The frequency shift can be assessed by exciting the system with a fixed excitation amplitude, and measuring the temporal evolution of the frequency of the fundamental nonlinear mode—which corresponds to the frequency ω in the PLL diagram in Fig. 1. Results show that the frequency increases with time (Fig. 11) which confirmed what has been observed in Fig. 10: the longer the excitation, the larger the frequency shift between forced and free regime. One interpretation of the frequency shift in Fig. 10 is the heating of the magnet as the duration or the amplitude of the excitation increases. It is worth mentioning that thermal losses due to the heating of the coil may impact the NNM damping factor and thus change the conservative and non-conservative NNM manifolds. However, we do think that these effects are not great enough to induce a change in the NNM damping—in fact no damping modification was measured between step ① and ②.

The influence of the coil heating on the NNM frequency is investigated by studying numerically the influence of a

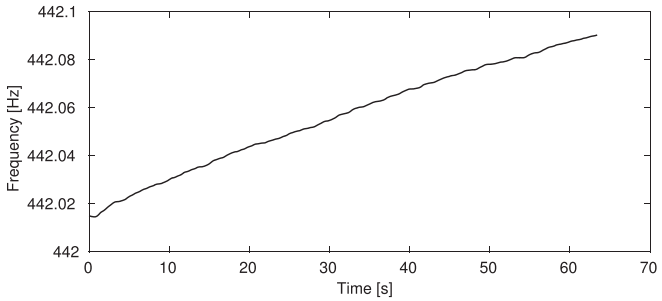

FIG. 11. Temporal evolution of the fundamental mode frequency when forcing the gong with a constant amplitude level 3.1 A.

local temperature increase on modal frequencies of a shallow spherical shell using finite element analysis. We assume that the conical edge of the gong imposes a nearly rigid boundary condition to the central vibrating section.[4] Consequently, we consider the central part of the gong as a clamped spherical shell of thickness h, diameter $D = 116\,\text{mm}$, and slope at the edge ψ [Fig. 12(a)]. The finite element code Cast3M (Ref. 36) is used with a thermo-mechanical conduction model discretized by COQ3 elements (six degrees-of-freedom for rotation and translation, and one thermal degree-of-freedom). The mechanical characteristics are those of the bronze: Young modulus $E = 110 \times 10^9\,\text{Pa}$, Poisson's ratio $\nu = 0.34$, density $\rho = 8560\,\text{kg m}^{-3}$, coefficient of thermal expansion $\delta = 1.6 \times 10^{-5}\ \text{K}^{-1}$ and thermal conductivity $K = 3.8\,\text{W m}^{-1}.\text{K}^{-1}$. The temperature of the shell edges T_e is set constant with $T_e = 20\,^\circ\text{C}$. Various temperatures T_c ranging from $T_c = 20\,^\circ\text{C}$ to $T_c = 26\,^\circ\text{C}$ are imposed at the center of the shell. The results for $t = 0.95\,\text{mm}$ are exposed in Figs. 12(a) and 12(b). The increase of the central section temperature results in a change of the fundamental mode frequency f_1 that depends on the angle ψ [Fig. 12(a)]. For plates and low curvature shells ($\psi < 0.14\,\text{deg}$), the fundamental frequency decreases with a temperature increase ($\Delta f_1 < 0$) [Fig. 12(b)]. In this case, the temperature increase leads to a dilatation of

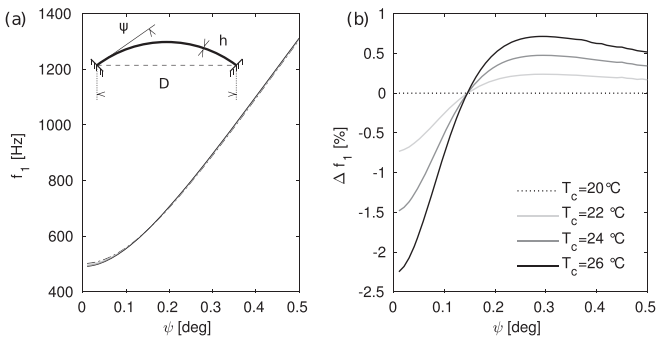

FIG. 12. Evolution of mode 1 frequency of a clamped spherical shell for a central temperature T_c ranging from 20 °C to 26 °C and a slope ψ ranging from 0.1° to 0.5°. (a) Frequency f_1 and (b) relative frequency variation Δf_1 of mode 1 as a function of slope ψ.

the mean surface of the shell that is blocked by the clamped boundary conditions, resulting in a decreasing of the linear stiffness of the shell (a softening effect), and consequently of the fundamental frequency. For more curved shells, with $\psi > 0.14$ deg, the dilatation leads to a deformation of the shell that increases its curvature, which has a stiffening effect, larger than the above cited softening effect. As a result, the fundamental frequency increases ($\Delta f_1 > 0$). Other simulations with several shell thicknesses h have been carried out, leading in each case to a limit value of ψ, that depends on h.

Note that our numerical model is designed without taking into account the residual stress induced by the manufacturing process, which is known to be used to tune the natural modes of vibration to improve the sound of the instrument.[37] We may assume that taking into account the coupling between this residual stress and the thermal effects may change the numerical results exposed in Fig. 12, however, it is not investigated in the present work. Moreover, the numerical results are in agreement with the experimental observations: in the present case of the *xiaoluo* gong, the temperature increase has a stiffening effect (Figs. 10 and 11), whereas for a less curved *daluo* gong tested in Ref. 25, a softening effect has been noticed. Those results are fully consistent with the above numerical study.

V. EFFECTS OF INTERNAL RESONANCES

A. Frequency-time analysis

Internal resonances are energy exchanges that occur between modes that are strongly coupled by geometrical nonlinearities.[2] They have been reported in numerous studies that concern the nonlinear behavior of beams,[38] plates,[35] shells,[13] and even other percussion instruments like large Chinese tam-tams[10] and steelpans.[12] In the case of the Chinese opera gongs, internal resonances have already been demonstrated using modal active control.[6]

As noticed in Sec. IV A, Fig. 7 suggests the presence of a 1:2 internal resonance between mode 1 whose frequency f_1 is such that $f_1(t) \in [380-447\,\text{Hz}]$, and modes 2 and 3 at $f_2 = 859$ Hz and $f_2 = 880$ Hz. For relatively small impact forces, the pitch glide is not so important but it is sufficient to make the second harmonic distortion reach the linear mode at 880 Hz [Fig. 7(b)]. As a result, a 1:2 internal resonance takes place between the fundamental mode and the mode at 880 Hz, and small frequency oscillations appear in both the fundamental mode and the second harmonic distortion. For high mallet

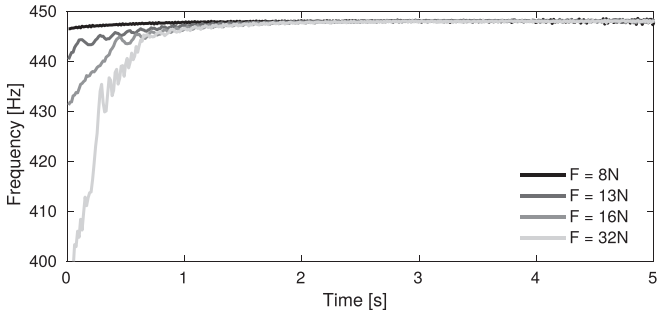

FIG. 13. Instantaneous frequency of the fundamental mode of the signals whose spectrograms are displayed in Fig. 7.

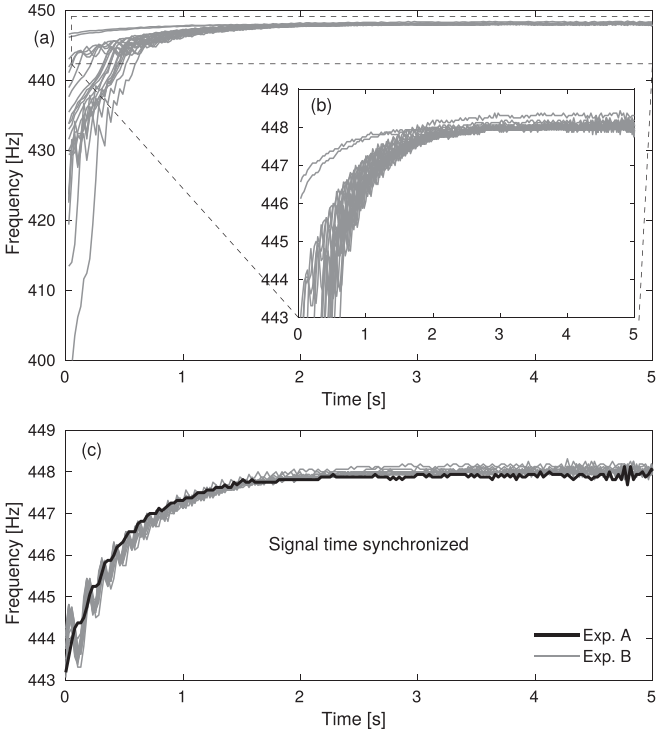

FIG. 14. (a) Pitch glides of the fundamental mode for the mallet strikes performed in experiment B. (b) Selection of the pitch glides in the frequency range 443−449 Hz. (c) Results of the temporal synchronization of the pitch glides displayed in (b). The nonlinear mode pitch glide of experiment A (single nonlinear mode excitation, black line) is also plotted.

momentum [Figs. 7(c) and 7(d)], the fundamental pitch glide is larger and a 1:2 internal resonance also takes place between the fundamental mode and the mode at 859 Hz. Note that the frequency oscillations are initiated in the fundamental mode when the frequency of the second harmonic distortion (black dot line) is equal to the frequency of the linear mode (red dot line)—the synchronization of these two events is clearly highlighted in Fig. 7(d). The frequency beats are more evident by only looking at the time evolution of the fundamental mode frequency (Fig. 13) of the spectrograms displayed in Fig. 7. When the frequency range of mode 1 is large—that is, when the impact force is sufficiently high—frequency beats occur when the upward pitch glide reaches $f_1 \sim 430$ Hz (impact force: 32N) and $f_1 \sim 440$ Hz (impact forces: 13N, 16N, and 32N). These frequency values are exactly half the frequency values of modes 2 and 3.

Strikingly, this result is observed regardless of the impact force, providing that it allows a pitch glide in the range 460−449 Hz. If the fundamental pitch glide of the mallet strikes performed in experiment B [Fig. 14(a)] are selected in the PLL frequency range 443−449 Hz [Fig. 14(b)], and are then time-synchronized and merged [Fig. 14(c)], then perfect synchronous frequency oscillations can be observed between them. Figure 14(c) also shows the frequency glide of the same nonlinear mode in the case of experiment A (single nonlinear mode excitation, solid black line). Contrary to the playing situation of experiment B, the frequency-time dependence of the fundamental mode in experiment A does not display any

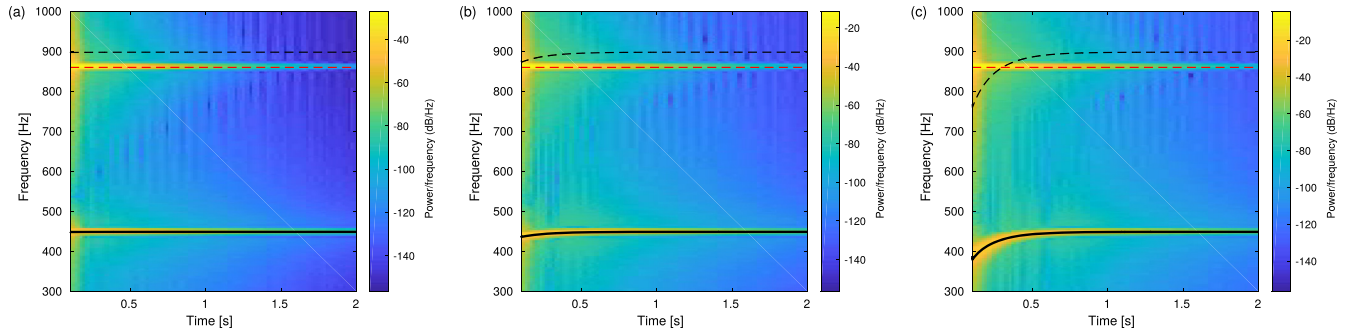

FIG. 15. (Color online) Spectrograms of the simulated displacement $u_1 + u_2$, along with the instantaneous frequency of mode 1 (solid black line) and mode 2 (dash red line), and the quadratic harmonic distortion of mode 1 (black dash line, plotted by multiplying by two the frequency of mode 1). For all the spectrograms no coupling is present ($\alpha = \beta = 0$). Initial values u_{20} and u_{10} for u_2 and u_1 are such that $u_{20} = 5 \times u_{10}$. (a) $u_{10} = 0.05$ mm, (b) $u_{10} = 0.30$ mm, (c) $u_{10} = 0.68$ mm.

frequency oscillations. This last result clearly highlights the limitation of a single nonlinear mode modeling for the description of the frequency-time dependency (pitch glide) in playing situation.

B. Simulations

The effect of internal resonances on the pitch glide are qualitatively investigated using a simulation of a two degree-of-freedom system coupled with quadratic nonlinear terms. A cubic term is added to the first oscillator in order to reproduce the pitch glide phenomenon, and modal viscous damping is assumed here. The normal form of a two degree-of-freedom system with a 1:2 internal resonance ($\omega_2 = 2\omega_1$) is[13]

$$\begin{aligned} &\ddot{u}_1 + 2\xi_1\omega_1\dot{u}_1 + \omega_1^2 u_1 + \tilde{\Gamma}_0 u_1^3 + \alpha u_1 u_2 = 0, \\ &\ddot{u}_2 + 2\xi_2\omega_2\dot{u}_2 + \omega_2^2 u_2 + \beta u_1^2 = 0. \end{aligned} \tag{10}$$

This two degree of freedom system aims at reproducing the 1:2 internal resonance between mode 1 and mode 2. The second 1:2 internal resonance reported in Sec. V A and implying mode 1 and mode 3 is not considered here for the sake of simplicity. The first oscillator corresponds to a nonlinear normal mode [Eq. (7)] with an added resonant quadratic coupling term. The second oscillator does not have any cubic nonlinear term because the frequency of mode 2 barely moves, as depicted in the experimental spectrograms (Fig. 7). The two quadratic coupling terms correspond to the resonant terms that cannot be canceled by the nonlinear change of variables [Eq. (3)] leading to the normal form. All other quadratic nonlinear terms have been canceled as they are non-resonant: they do not drive one of the oscillators close to its resonance and are therefore not important in the system dynamics.

The simulation parameters are $\omega_1 = 2\pi \times 447\,\text{rad.s}^{-1}$, $\omega_2 = 2\pi \times 859\,\text{rad.s}^{-1}$, $\xi_1 = \xi_2 = 10^{-3}$, and $\tilde{\Gamma}_0 = -6.7 \times 10^6$ $\text{mm}^{-2}\text{s}^{-2}$. The value of the linear parameter ξ_1 is extracted from a previous study.[6] The value of $\tilde{\Gamma}_0$ is estimated by measuring the backbone curve with the vibrometer pointing at the center of the instrument. This measure leads to a value of $\tilde{\Gamma}_0$, which is different from the value Γ_0 measured in Sec. IV B, as explained at the end of Sec. II A. The nonlinear quadratic coefficients α and β are not known *a priori*. An extensive presentation of the influence of α and β would be too tedious, but some interesting values can be extracted in order to assess their influence on the system dynamics Eq. (10). When $\alpha = \beta = 0$, no nonlinear coupling is present between the two oscillators, and the system dynamics follows the traditional Duffing response. This is confirmed by looking at the spectrograms of the simulated displacement $u_1 + u_2$ in Fig. 15. The influence of the nonlinear parameter α is investigated while keeping the nonlinear parameter β to zero. If $\alpha < 10^4\,\text{mm}^{-1}\text{s}^{-2}$, no influence on the pitch glide if observed. In Fig. 16, the spectrogram of the simulated displacement $u_1 + u_2$ is plotted for increasing values of α in high vibration amplitude (pitch glide range $\sim$50 Hz). One can see that increasing the α parameter leads to a slope discontinuity in the pitch glide of the fundamental mode, as noticed in the experimental results in Figs. 6 and 7. The effect of

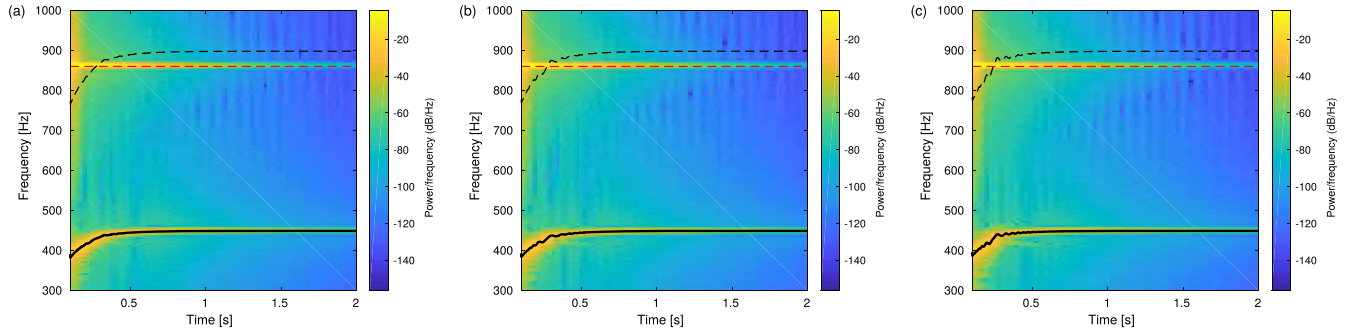

FIG. 16. (Color online) Spectrograms of the simulated displacement $u_1 + u_2$ for increasing α values, with parameters $\beta = 0\,\text{mm}^{-1}\text{s}^{-2}$, $u_{10} = 0.68$ mm, and $u_{20} = 5 \times u_{10}$. (a) $\alpha = 3 \times 10^4\,\text{mm}^{-1}\text{s}^{-2}$, (b) $\alpha = 5 \times 10^4\,\text{mm}^{-1}\text{s}^{-2}$, (c) $\alpha = 8 \times 10^4\,\text{mm}^{-1}\text{s}^{-2}$. Legend is the same as in Fig. 15.

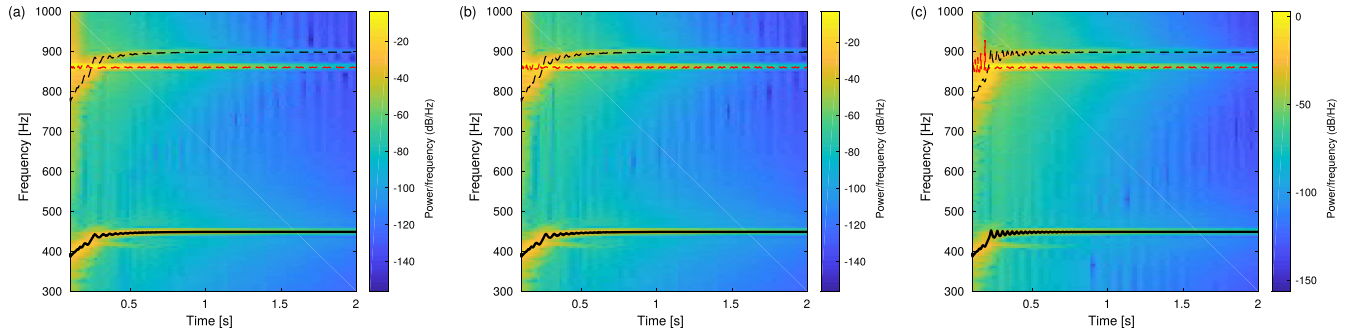

FIG. 17. (Color online) Spectrograms of the simulated displacement $u_1 + u_2$, with parameters $\alpha = 8 \times 10^4\,\mathrm{mm^{-1}s^{-2}}$, $u_{10} = 0.30\,\mathrm{mm}$, and $u_{20} = 5 \times u_{10}$. (a) $\beta = 5 \times 10^6\,\mathrm{mm^{-1}s^{-2}}$, (b) $\beta = 10^7\,\mathrm{mm^{-1}s^{-2}}$, (c) $\beta = 5 \times 10^7\,\mathrm{mm^{-1}s^{-2}}$. Legend is the same as in Fig. 15.

the change of the β parameter is illustrated in Fig. 17, where spectrograms of the system response for increasing β values are displayed. The first direct effect of the β term is to change the behavior of the second oscillator with the source term βu_1^2. The modification of the second oscillator causes a second effect by modifying the first oscillator response with the term $\alpha u_1 u_2$. The greater β is, the greater are the energy exchanges between the two oscillators [Fig. 17(c)]. However, an excessive increase of β also leads to a complex response in the second oscillator, which is not the case in the experiments [see Fig. 7(d)].

Figure 18 shows a qualitative correct choice of α and β for the description of the experimental results: $\alpha = 8 \times 10^4\,\mathrm{mm^{-1}s^{-2}}$ and $\beta = 3 \times 10^6\,\mathrm{mm^{-1}s^{-2}}$. Note that this choice has been empirically identified, and reproduce the experimental results only qualitatively—for example, the temporal duration of the pitch glide in the experiments (Fig. 7) and in the simulations (Fig. 18) differs by a factor of 4. However, these simulations are able to reproduce the slope discontinuity as well as the oscillations in the pitch glide. Moreover, note that the oscillations start when the frequency of the second harmonic distortion is equal to the frequency of the mode at 860 Hz. This decisively points out the role of internal resonances in the pitch glide of the gong fundamental mode.

VI. CONCLUSION

This paper investigates a reduced order model for the description of the fundamental pitch glide of a Chinese opera gong displaying an ascendant pitch glide. The study relies on the nonlinear modes formalism and the measure of the backbone curve and frequency-time relationship of the fundamental nonlinear mode, in free vibration regime. Two experiments were carried out. The first experiment (experiment A) investigated a single nonlinear mode modeling by measuring the backbone curve and the frequency-time dependency of the fundamental nonlinear mode *alone*, with no other nonlinear modes excited during the experiment. The experimental and original protocol combines the use of PLL setup, which is traditionally performed in forced vibration, and free decay vibration on a nonlinear mode manifold, which is the main idea of nonlinear phase resonance testing. The second experiment (experiment B) performed the same measurements than the first experiment, this time by striking the gong with a mallet, allowing for a multi-modal excitation that leads to internal resonances between the nonlinear fundamental mode and higher frequency modes.

The comparison of the two experiments' results show that (i) in a small frequency range around the fundamental modal frequency (∼447 Hz), the single nonlinear mode model is able to reproduce the frequency-amplitude dependency (i.e., the pitch glide) of the fundamental mode in playing situation; (ii) the frequency-time analysis of the fundamental nonlinear mode reveals that internal resonances appear between the fundamental mode and other linear modes. These internal resonances happen when the frequency of the fundamental mode, gliding upward, is the half of the frequency of two other linear modes at 859 and 880 Hz. The energy exchanges inherent to these resonances are highlighted by frequency beats in the fundamental mode pitch glide. This latter result was qualitatively demonstrated by simulating a quadratically coupled two-degree-of-freedom system fulfilling a 1:2

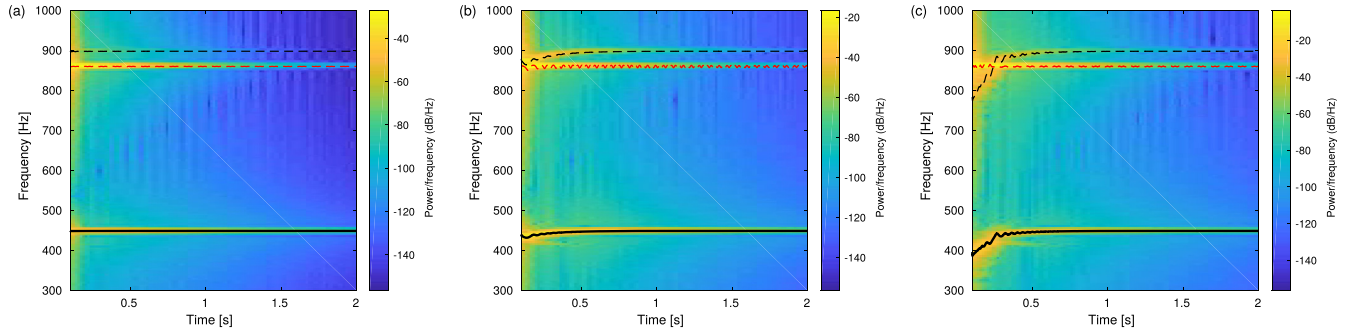

FIG. 18. (Color online) Spectrograms of the simulated displacement $u_1 + u_2$, with parameters $\alpha = 8 \times 10^4\,\mathrm{mm^{-1}s^{-2}}$, $\beta = 3 \times 10^6\,\mathrm{mm^{-1}s^{-2}}$, $u_{20} = 5u_{10}$. (a) $u_{10} = 0.05\,\mathrm{mm}$, (b) $u_{10} = 0.30\,\mathrm{mm}$, and (c) $u_{10} = 0.68\,\mathrm{mm}$. Legend is the same as in Fig. 15.

resonance relationship ($\omega_2 = 2\omega_1$); (iii) frequency shifts appear when measuring the *backbone curves*; they were interpreted as thermal effects due to the heating of the magnet used for the excitation. These thermal effects were highlighted by a numerical study investigating the influence of temperature on the fundamental mode of a clamped spherical shell. Results show that the frequency variation can be either negative or positive, depending on the competition between a compression effect and the curvature increase.

Finally, this study experimentally highlights the interaction between the pitch glide phenomenon and internal resonances in free vibration regime. It also provides the first step for the detailed comprehension of the pitch glide in Chinese gongs. In the case of the *xiaoluo*, a three modes model could easily be determined by experimentally identifying the nonlinear coupling coefficients of each 1:2 internal resonance that have been highlighted in the study, as previously made for example in Ref. 12.

[1]N. Fletcher and T. Rossing, *The Physics of Musical Instruments* (Springer-Verlag, London, 1998).
[2]A. H. Nayfeh and D. T. Mook, *Nonlinear Oscillations*, (Wiley-VCH, Weinheim, 1995), pp. 1–720.
[3]T. D. Rossing and N. H. Fletcher, "Nonlinear vibrations in plates and gongs," J. Acoust. Soc. Am. **73**, 345–351 (1983).
[4]N. H. Fletcher, "Nonlinear frequency shifts in quasispherical-cap shells: Pitch glide in Chinese gongs," J. Acoust. Soc. Am. **78**, 2069–2073 (1985).
[5]G.-C. Tsai, B.-T. Wang, Y.-S. Lee, and Z.-W. Chang, "Study of vibration and sound characteristics of a copper gong," J. Chin. Inst. Eng. **28**(4), 713–719 (2005).
[6]M. Jossic, A. Mamou-Mani, B. Chomette, D. Roze, F. Ollivier, and C. Josserand, "Modal active control of Chinese gongs," J. Acoust. Soc. Am. **141**, 4567–4578 (2017).
[7]K. Legge and N. Fletcher, "Nonlinearity, chaos, and the sound of shallow gongs," J. Acoust. Soc. Am. **86**(6), 2439–2443 (1989).
[8]C. Touzé and A. Chaigne, "Lyapunov exponents from experimental time series: Application to cymbal vibrations," Acust. Acta Acust. **86**(3), 557–567 (2000).
[9]O. Thomas, C. Touzé, and A. Chaigne, "Nonlinear behavior of gongs through the dynamics of simple rods systems," in *Proceedings of the International Symposium on Musical Acoustics* 1, Perugia, Italy (September 10–14, 2001), pp. 179–178.
[10]A. Chaigne, C. Touzé, and O. Thomas, "Nonlinear vibrations and chaos in gongs and cymbals," Acoust. Sci. Technol. **26**, 403–409 (2005).
[11]M. Monteil, C. Touzé, O. Thomas, and S. Benacchio, "Nonlinear forced vibrations of thin structures with tuned eigenfrequencies: The cases of 1:2:4 and 1:2:2 internal resonances," Nonlinear Dyn. **75**, 175–200 (2014).
[12]M. Monteil, O. Thomas, and C. Touzé, "Identification of mode couplings in nonlinear vibrations of the steelpan," Appl. Acoust. **89**, 1–15 (2015).
[13]O. Thomas, C. Touzé, and A. Chaigne, "Non-linear vibrations of free-edge thin spherical shells: Modal interaction rules and 1: 1: 2 internal resonance," Int. J. Solids Struct. **42**, 3339–3373 (2005).
[14]C. Touzé, O. Thomas, and A. Chaigne, "Hardening/softening behaviour in non-linear oscillations of structural systems using non-linear normal modes," J. Sound Vib. **273**, 77–101 (2004).
[15]C. Touzé and O. Thomas, "Non-linear behaviour of free-edge shallow spherical shells: Effect of the geometry," Int. J. Non-Linear Mech. **41**(5), 678–692 (2006).
[16]C. Touzé and M. Amabili, "Nonlinear normal modes for damped geometrically nonlinear systems: Application to reduced-order modelling of harmonically forced structures," J. Sound Vib. **298**(4), 958–981 (2006).
[17]L. Jezequel and C. Lamarque, "Analysis of non-linear dynamical systems by the normal form theory," J. Sound Vib. **149**(3), 429–459 (1991).
[18]M. F. Platten, J. R. Wright, G. Dimitriadis, and J. E. Cooper, "Identification of multi-degree of freedom non-linear system using an extended modal space model," Mech. Syst. Signal Process. **23**, 8–29 (2009).
[19]M. Peeters, G. Kerschen, and J. C. Golinval, "Dynamics testing of nonlinear vibrating structures using nonlinear normal modes," J. Sound Vib. **330**(3), 486–509 (2011).
[20]J. Sieber and B. Krauskopf, "Control based bifurcation analysis for experiments," Nonlinear Dyn. **51**(3), 365–377 (2008).
[21]L. Renson, A. Gonzalez-Buelga, D. A. W. Barton, and S. A. Neild, "Robus identification of backbone curves using control-based continuation," J. Sound Vib. **367**, 145–158 (2016).
[22]S. Mojrzisch and J. Twiefel, "Phase-controlled frequency response measurement of a piezoelectric ring at high vibration amplitude," Arch. Appl. Mech. **86**(10), 1763–1769 (2015).
[23]S. Peter, R. Riethmüller, and R. I. Leine, "Tracking of backbone curves of nonlinear systems using phase-locked-loop," Nonlinear Dyn. **1**, 107–120 (2016).
[24]V. Denis, M. Jossic, A. Renault, C. Giraud-Audine, and O. Thomas, "Robust measurement of backbone curves of a nonlinear piezoelectric beam," *ENOC 2017*, Budapest, Hungary (June 25−30, 2017).
[25]V. Denis, M. Jossic, C. Giraud-Audine, B. Chomette, A. Renault, and O. Thomas, "Identification of nonlinear modes using phase-locked-loop experimental continuation," Mech. Syst. Signal Process. **106**, 430–452 (2018).
[26]S. W. Shaw and C. Pierre, "Nonlinear normal modes and invariant manifolds," J. Sound Vib. **150**(1), 170–173 (1991).
[27]G. Kerschen, M. Peeters, J.-C. Golinval, and A. F. Vakakis, "Nonlinear normal modes, Part I: A useful framework for the structural dynamicist," Mech. Syst. Signal Process. **23**(1), 170–194 (2009).
[28]J. R. Wright, J. E. Cooper, and M. J. Desforges, "Normal-mode force appropriation—Theory and applications," Mech. Syst. Signal Process. **13**(2), 217–240 (1999).
[29]M. Peeters, G. Kerschen, and J. C. Golinval, "Modal testing of nonlinear vibrating structures based on nonlinear normal modes: Experimental demonstration," Mech. Syst. Signal Process. **25**(4), 1227–1247 (2011).
[30]J. M. Londono, S. A. Neild, and J. E. Cooper, "Identification of backbone curves of nonlinear systems from resonance decay responses," J. Sound Vib. **348**, 224–238 (2015).
[31]D. A. Ehrhardt and M. S. Allen, "Measurement of nonlinear normal modes using multi-harmonic stepped force appropriation and free decay," Mech. Syst. Signal Process. **76–77**, 612–633 (2016).
[32]R. E. Best, *Phase-Locked Loops—design, Simulation and Applications* (McGraw Hill, New York, 2007), 6th ed.
[33]I. J. Sokolov and V. I. Babitsky, "Phase control of self-sustained vibration," J. Sound Vib. **248**(4), 725–744 (2001).
[34]J. Twiefel, M. Klubal, C. Paiz, S. Mojrzisch, and H. Krüger, "Digital signal processing for an adaptive phase-locked loop controller," Proc. SPIE **6926**, 69260A–69260A-12 (2008).
[35]O. Thomas, C. Touzé, and A. Chaigne ,"Asymmetric non-linear forced vibrations of free-edge circular plates, part 2: Experiments," J. Sound Vib. **265**(5), 1075–1101 (2003).
[36]Information on Cast3M available at http://www-cast3m.cea.fr (Last viewed on 13 May 2018).
[37]N. McLachlan, "Tuning natural modes of vibration by prestress in the design of a harmonic gong," J. Acoust. Soc. Am. **131**(1), 926–934 (2012).
[38]F. Mangussi and D. H. Zanette, "Internal resonance in a vibrating beam: A zoo of nonlinear resonance peaks," PLoS One **11**(9), e0162365 (2016).